Lab on a Chip

Dynamic Article Links

Cite this: *Lab Chip*, 2011, **11**, 2447

www.rsc.org/loc

PAPER

Inkjet-like printing of single-cells

Azmi Yusof,[a] Helen Keegan,[bc] Cathy D. Spillane,[bc] Orla M. Sheils,[b] Cara M. Martin,[bc] John J. O'Leary,[bc] Roland Zengerle[ad] and Peter Koltay*[ae]

Received 1st March 2011, Accepted 10th May 2011
DOI: 10.1039/c1lc20176j

Cell sorting and separation techniques are essential tools for cell biology research and for many diagnostic and therapeutic applications. For many of these applications, it is imperative that heterogeneous populations of cells are segregated according to their cell type and that individual cells can be isolated and analysed. We present a novel technique to isolate single cells encapsulated in a picolitre sized droplet that are then deposited by inkjet-like printing at defined locations for downstream genomic analysis. The single-cell-manipulator (SCM) developed for this purpose consists of a dispenser chip to print cells contained in a free flying droplet, a computer vision system to detect single-cells inside the dispenser chip prior to printing, and appropriate automation equipment to print single-cells onto defined locations on a substrate. This technique is spatially dynamic, enabling cell printing on a wide range of commonly used substrates such as microscope slides, membranes and microtiter plates. Demonstration experiments performed using the SCM resulted in a printing efficiency of 87% for polystyrene microbeads of 10 μm size. When the SCM was applied to a cervical cancer cell line (HeLa), a printing efficiency of 87% was observed and a post-SCM cell viability rate of 75% was achieved.

1. Introduction

The ability to isolate cell subpopulations and single cells from heterogeneous cell populations has enormous potential in areas such as diagnostics, therapeutics and cell biology. Cells of interest are often surrounded by a background of biological noise, for example in a complex cell culture, a biological sample or in a microbial biofilm. In diagnostics, the isolation of individual cellular components from clinical specimens is commonplace. An example of this is the fractionation of blood components: plasma, erythrocytes, leucocytes and platelets. Recently, there has been a drive to miniaturise cell sorting systems into lab-on-a-chip devices; *e.g.* blood-on-a-chip device.[1] Despite these advances, there is still a need to develop systems that can isolate rare single cells in a milieu of cellular material. In cancer diagnostics, the isolation of circulating tumour cells may be important for non-invasive monitoring of cancer patients[2] and in the perinatal setting, the isolation of foetal cells from the maternal circulation may provide insights into rare genetic developmental disorders.[3] In therapeutics, the ability to isolate progenitor autologous stem cells from host tissue may drive forward whole cell therapeutics for the treatment of degenerative conditions.[4]

Conventional cell sorting techniques such as continuous flow-cytometry and fluorescence-activated cell sorting (FACS) or magnetic activated cell sorting (MACS) are often used in cell biology. The scatter and fluorescent data that these methods produce can yield significant information on cell type, size, surface–protein expression, ploidy and fluorescent marker signature.[5] However, their use requires prior knowledge of a cell's phenotypic characteristics and such cell sorting systems do not lend themselves to the isolation of non-labelled, unaltered, native cells for single cell specific, post-cell-sorting, genome-wide analysis. Furthermore, fluid shear stresses combined with the addition of labels may render cells non-viable following the use of such methods. Thus, the ability to understand cell behaviour at a molecular level often rests on the availability of techniques to isolate and collect viable single-cells for subsequent downstream experiments and genetic analysis. Although flow-cytometry is powerful and capable of performing high-throughput single cell data collection,[5] its capacity to decipher the spatio-temporal information of an individual single-cell is limited.

Current methods for cell patterning include soft lithographic techniques such as micro-contact printing,[6–10] where cells adhere to selectively biochemically treated areas and form the printed pattern, and microwell trapping,[10–12] where single-cell entrapment occurs in micropores or a defined diameter after deposition

[a]*Laboratory for MEMS Applications, Department of Microsystems Engineering (IMTEK), University of Freiburg, Germany. E-mail: koltay@imtek.uni-freiburg.de*
[b]*University of Dublin, Trinity College, Ireland*
[c]*Coombe Women and Infants University Hospital, Dublin, Ireland*
[d]*Centre for Biological Signalling Studies (BIOSS), University of Freiburg, Germany*
[e]*Biofluidix GmbH, Germany*

of a cell suspension before the excess medium is removed. These direct contact strategies of seeding single cells offer little flexibility in cell size variation, pattern shape or spacing and they are prone to cross-contamination between the immobilized cells. Therefore, considerable efforts have been made to develop non-contact "cell printing" methods for seeding cells onto substrates. It has been shown that cells can be encapsulated within a free flying microdroplet and then printed precisely onto a substrate using an inkjet printer,[13] by acoustic droplet generation[14] and by electrohydrodynamic spraying.[15] Chinese Hamster Ovarian (CHO) cells have been printed using a thermal inkjet printer with post-printing survival rates of approximately 90%.[16] Such non-contact strategies provide unique advantages over arraying cells on spatially patterned substrates, such as the opportunity to develop 3-dimensional cellular structures[17] of defined cell-type composition. The controlled deposition of single cells is however an essential requirement for printing single cell arrays or for patterning different cell types in the attempt to construct artificial tissues with high resolution. Even though obtaining single cells in each printed spot is possible by such inkjet printing methods, when the cell density in the suspension is reduced,[18–20] the overall performance is low and the occurrence of droplets containing only one single cell has to be considered as random.

This paper reports on the development of a novel device which enables a controlled "one-droplet-one-cell"-like printing of single cells, referred to as the single-cell-manipulator (SCM). The described SCM provides a platform for isolating single cells while also automatically delivering them into predefined positions for virtually any purpose. In this study, the capability of the SCM to print single particles (polystyrene microbeads) and mammalian cells (HeLa cells) onto different substrates, in particular glass slides and microwell plates, with minimal loss of cell viability is demonstrated.

2. Materials and methods

2.1 Single cell manipulator (SCM) system

The SCM has three main functions: (i) isolation of a single cell from a cell suspension, (ii) generation of droplets containing single cells only and (iii) automated placement of single cells onto a substrate. Fig. 1(a) shows the components of SCM system. The core element of the system is a droplet generator that creates free flying droplets from a cell suspension, allowing for optical monitoring of the cell distribution inside the droplet generator prior to dispensing. In the presented case a dispenser chip[21] made from silicon and glass with standard microfabrication technology and driven by a piezo stack actuator was used. This chip as shown in Fig. 1(d) (inset) is similar to piezoelectric inkjet print heads in a "drop on demand" mode. The main difference of this new technology to the current inkjet technology is the larger and adjustable droplet volume, the adjustable droplet velocity and even more importantly the transparent glass cover of the chip that makes the nozzle accessible for optical view. By variation of the electrical signal driving the piezo, droplets of 150–800 pl can be generated (see graph in Fig. 1(d)). Because the nozzle surface condition affects the ability for the dispenser to generate the droplet, to avoid nozzle wetting a hydrophobic coating has been applied on the nozzle surface. A charged-couple device (CCD) camera was used for optical imaging of the nozzle section of the chip to detect single cells prior to dispensing. This region of interest (ROI) inside the dispenser chip is observed by a computer vision system which can detect cell occupancy at the nozzle.

In order to control the number of cells contained within one ejected droplet, instead of random dispensing of single cells like reported previously using inkjet technology, two additional features were incorporated into the system: (i) an optical particle detection mechanism and (ii) a sorting algorithm. While the detection mechanism serves to determine the existence of single cells within the ROI in close proximity to the dispenser nozzle, the sorting algorithm will ensure that only single cells are dispensed and delivered to the prescribed location.

2.2 Droplet separation and detection algorithms

While a detailed description of the optical detection system and algorithm is given below, the sorting algorithm should be described first, as follows: first the droplet generator is triggered to dispense one droplet into a waste reservoir by appropriately positioning the dispenser over the waste position. For the dispensed droplet the status of the cell distribution inside the region of interest (ROI) is recorded by the optical system and the number of cells that will be expelled with the next droplet is predicted by the image recognition algorithm. In the simplest case, the sensing region (in this case ROI) is defined by the volume that will be expelled to create the next droplet.

In this case, the number of cells inside the ROI is the measurement which determines the number of cells to be dispensed in the subsequent droplet. The number of cells in the ROI can be easily obtained from the camera image taken by the optical system by automatic image processing as described below, to yield the number of cells in the ROI ($N = 0, 1, 2, \ldots$). If the measurement of the cell distribution inside the ROI yields any number different from one (*i.e.* $N \neq 1$), then the next droplet is delivered to the waste position and a new camera image is taken. If the measurement yields exactly one cell ($N = 1$), then the dispenser is moved to the target position by mechanical movement of the stages and the subsequent droplet is printed at the target position. Once the droplet containing the cell has been delivered to the target position, the dispenser moves back to the waste position and the algorithm starts again from the beginning.

To realize the detection of cells in the ROI, an optical setup as shown in Fig. 1(a) was used: the nozzle was illuminated by a cold lamp (KL-1500-LCD; Leica, Germany) and the camera (UI-2230C; IDS, Germany) was furnished with a zoom objective (Opto; Sonderbedarf, Germany) to record images of the nozzle section as shown in Fig. 1(c). A real-time automatic particle detection algorithm[22] written in Visual Studio 2005 (Microsoft Corporation) was applied to automatically analyse the images within the ROI. This image-processing algorithm[23] simply works by differencing two consecutive image frames acquired by the camera that were set at grey scale level. Sequentially, an image segmentation procedure is performed above the threshold grey scale value to unveil the foreground. The image segmentation results in a new binary image, which reveals the foreground that shows changes in the subsequent image frame. The existence of particles or cells (if any) is represented on the binary image as

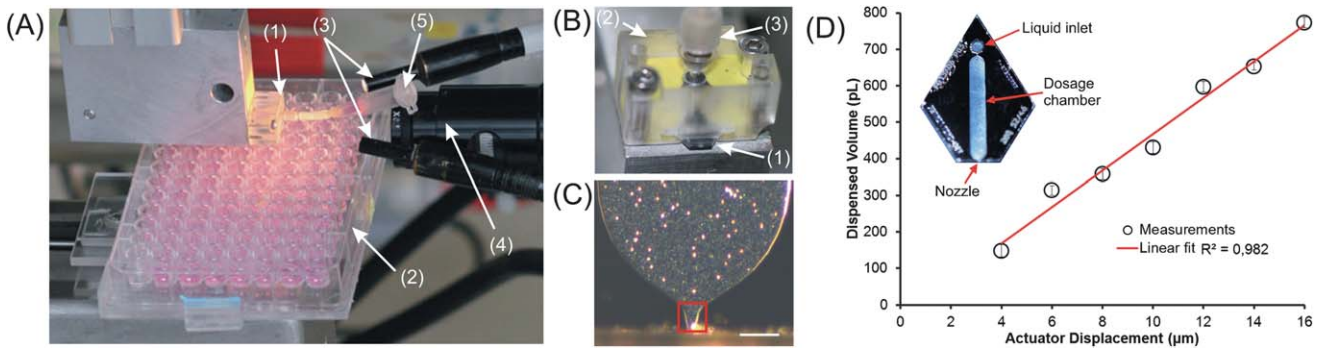

Fig. 1 (a) Single-cell-manipulator (SCM) system for printing single-cells consists of (1) dispenser chip mounted to the aluminium case that hosts the piezo-stack actuator, (2) target for single-cell printing (*e.g.* 96 well plate) mounted on motorized linear stage, (3) external illumination, (4) objective of a CCD camera for image recognition and cell detection and (5) reservoir. (b) Enlarged view of dispenser chip assembly (1) using transparent PMMA for mechanical fixture (2) and fluidic connection (3). (c) Image from a CCD camera focused on the nozzle showing HeLa cells approaching the nozzle orifice. The red square marks the ROI or sensing region from where the motion detection algorithm works to detect single-cells. Scale bar, 100 µm. (d) Dispenser chip fabricated from silicon/glass (Inset). The graph shows the dispensed droplet volume for deionized water generated by the dispenser chip at different piezo actuator displacement.

bright spots. To further refine the detection capability, an additional blob detection algorithm[23] step was added to count the number of particles or cells existing within the ROI. Based on this information, a prediction can be made, whether (i) a single cell or (ii) any other number of cells will be ejected with the subsequent dispensing step. A droplet containing a single cell is predicted for subsequent dispensing, if exactly one cell is detected in the ROI.

2.3 Cell culture

HeLa cells (ATCC CCL-2) were grown in culture media (MEM Eagle; Lonza Switzerland) supplemented with serum, penicillin, streptomycin (Invitrogen) and amino acids (Lonza, Switzerland) using a standard incubation environment (37 °C and 5% CO_2). Cells were harvested after reaching 80% confluence and then washed, trypsinised, centrifuged and re-suspended to produce a cell suspension at appropriate cell concentration. The cell suspension was aliquoted and a viability test was performed using Trypan Blue staining. Cells suspensions used for experiments exhibited an average of 98 ± 1% viable cells prior to the experiment. The cells were trypsinised and reseeded every 2 to 3 days.

2.4 Cleaning and sterilizing the chip

Upon fitting the dispenser chip into the SCM system, the following procedure was performed to ensure aseptic conditions inside the dispenser chip. Firstly, 15 µl ethanol solution (70% v/v) was pipetted into the reservoir and the dispenser was driven at high frequency dispensing mode until the solution in the reservoir was depleted. Subsequently, 15 µl cell culture medium was loaded and again the dispenser was driven at high frequency dispensing mode until the solution in the reservoir was depleted. Finally, 20 µl cells suspension was pipetted into the reservoir and continuous dispensing was performed until first cells were observed flowing through the nozzle area (visualized through the camera). From this point on, the SCM was ready to perform single-cell printing as described above. This cleaning procedure was carried each time before a new sample was loaded. The dispenser chip can be used multiple times if it is properly cleaned after use by flushing the fluid channel with deionized water several times. Upon cleaning, the chip was sterilized by autoclaving at 120 °C for 20 minutes and stored for subsequent use.

2.5 Printing on glass slides

Standard microscope glass slides (Carl Roth, Germany) were soaked in NaOH (1 M) solution overnight. The slides were washed thoroughly and rinsed at least three times with filtered water and finally, dried using compressed nitrogen gas. 50 coordinate positions were programmed on the graphical user interface (GUI) of the *x*–*y*-axis system (BioSpot 160, BioFluidix Freiburg, Germany) to give 10 × 5 arrays of printed spots at 500 µm centre-to-centre distance. The buffer solutions were loaded into the reservoir as described above and polystyrene-beads (Gerlinder Kisker; Germany) or cells were printed automatically using the hardware and algorithm. The glass slides were inspected under a bright field microscope and the polystyrene-beads or cells in each printed spot were counted manually. The bead/cell dispensing efficiency was determined by counting the number of beads or cells filled in individual printed spots divided by the total number of printed spots.

2.6 Cell printing in 96-well microplate and growth monitoring

Cells were printed into the wells of a NUNC 96 well flat bottom plates (NUNC; VWR, Germany). Each dataset consisted of 40 wells (utilized 4 rows and 10 columns). The first row was divided into two sections with 5 wells each identified as "control A" and "control B". The remaining wells (30 wells, in row 2 to 4) were identified as "single-cell". All 40 wells were prepared by adding 30 µl culture media into each well. For the "control B" and "single-cell" wells, the coordinates for printing were programmed according to the well positions using the GUI of the *x*–*y*-axis system.

In the "control A" wells, 1 µl cell suspension was pipetted manually. In the "control B" wells, 20 dispenses of 400 pl

droplets were delivered using the SCM and identical dispensing parameters like for the single cell dispensing but without controlling nor determining the number of cells. Finally, automated single cell printing into the remaining 30 wells was performed. After seeding the cells, each well was inspected under the microscope and the number of cells in each well was counted. The seeded well plates were returned to the incubator at 37 °C temperature and 5% CO_2 for one week. The wells were inspected regularly to monitor and count the cells accordingly. The yield of single cell survival was determined by dividing the total number of single cells that showed division in a well after day 2 by the total number of wells successfully populated with single cells. The cell culture media were changed every two days.

3. Results

3.1 Single-particle micro-array

The first experimental evaluation of the SCM performance was carried out using polystyrene microbeads of 10 μm diameter as a surrogate for biological cells. The main objective in this first experiment was to deposit droplets containing single particles onto a glass substrate and to determine suitable parameters for the detection and sorting algorithms. In order to obtain a good performance *i.e.* dispensing efficiency, the sensing region (referred to as the Region of Interest—ROI) is the most sensitive element to be considered. Determining the appropriate size and location of the ROI became a crucial task since the flow path of cells or particles inside the dispenser chip depends on many parameters like for example liquid flow velocity as well as size, position and drag coefficient of the particle.

As a first estimate to predict whether a cell or particle inside the chip will be expelled with the subsequent dispensing, the liquid volume inside the chip corresponding to the dispensed droplet volume was considered. The liquid volume depleted from the nozzle to produce a droplet corresponds to the surface area bounded by the trapezoidal shaped nozzle times the channel's depth (which is in the present case 40 μm). Determining the surface area eventually leads to a first estimate for the size of the ROI. To estimate this surface area, the measured droplet volume generated by the dispenser chip at 400 pl (see gravimetric measurement in Fig. 1(d)) was mapped onto the surface area of the dispenser chip close to the nozzle. The resulting shape is displayed in Fig. 2(a) as blue area B. The corresponding image size acquired by the image analysis system is displayed as a red rectangular sector in Fig. 2(a) upstream of the dispenser chip nozzle.

To determine the suitability of the estimated ROI for the given purpose, an experimental comparison with one larger and one smaller image differing by 20% in area size was performed (see red dashed lines and resulting blue shapes A and C in Fig. 2(a)). Experiments were performed by printing polystyrene beads onto glass slides using the different ROI marked with A, B and C in Fig. 2(a) and determining the dispensing efficiency by microscopic evaluation of the printed patterns. The so-called "dispensing efficiency" is defined by the number of spots containing one single particle divided by the total number of spots printed onto the substrate. This figure was used as a measure to determine the efficiency of the corresponding ROI and later on to study the influence of other parameters on the process.

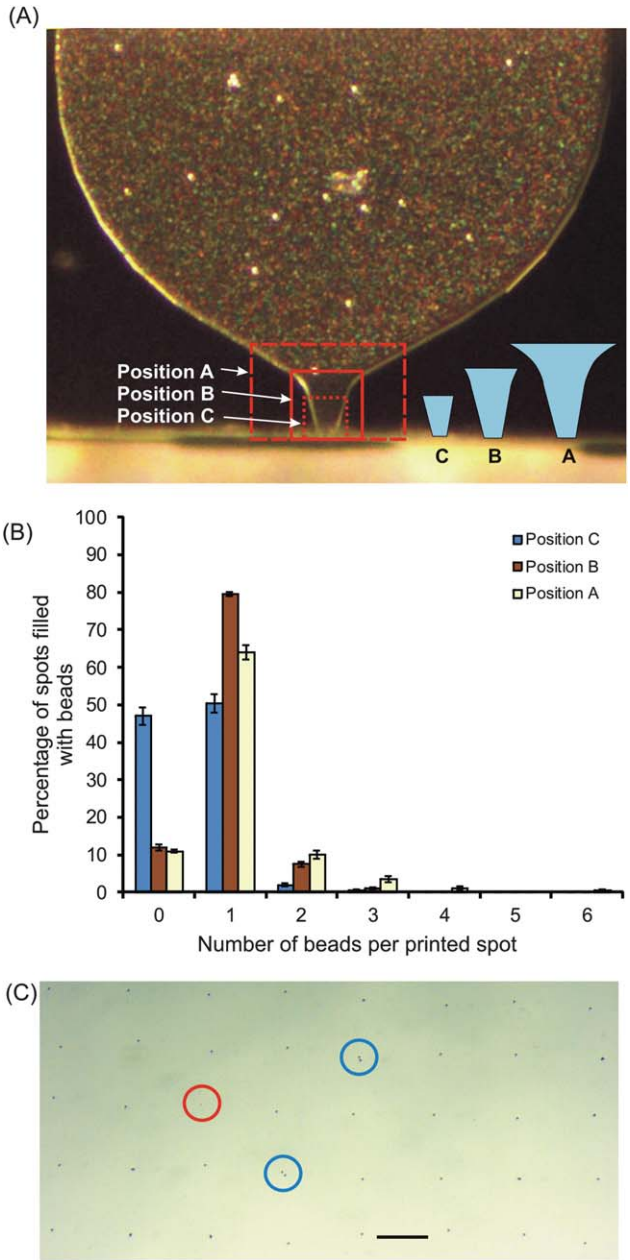

Fig. 2 (a) Definition of the location of the detection region or the region of interest (ROI). The red square sectors represent the ROI inside the dispenser chip that act as the sensing region. Calculated ROI position (position B) is equivalent to 400 pl liquid volume reside within the nozzle perimeter. Two different ROIs (positions A and C) were selected with a size that is different by 20% compared to the ROI at position B. (b) The dispensing efficiency shows a significant dependence of the ROI size (A, B or C), data correspond to a median from 50 printed spots. (c) Polystyrene beads printed onto glass slide (ROI position B). Unmarked spots contain single polystyrene bead, the red circle marks for void spot and blue circles highlight spots that are filled with more than a single polystyrene bead. Scale bar 250 μm.

For the first experiment, a buffer suspension at 2.6×10^4 particles per ml was prepared by suspending polystyrene beads (diameter 10 μm) into deionised water. This solution was then

supplied to the reservoir connected to the dispenser chip and printing was executed to generate 50 spots on a glass slide (10 × 5 array spots with 500 μm centre-to-centre distance). Notably, single polystyrene bead arrays could be successfully printed on the glass substrate as shown in Fig. 2(c).

The yield of spots occupied with single particles of about 80% was much higher than in any previous study reported in the literature by straightforward inkjet printing.[14,18,20,24] However, the dispensing efficiency does depend on the size and location of the ROI (as shown in Fig. 2(b)). For the droplet volume of 400 pl, the best dispensing efficiency was achieved with the ROI area B for all considered particle concentrations at an average dispensing efficiency of 80%. A larger ROI (type A) produces more spots occupied with more than one cell, while a smaller ROI (type C) produces more void spots containing no particles. On the basis of these findings, the ROI of type B and a corresponding droplet volume of 400 pl were used for subsequent experiments.

3.3 Effects of varying the buffer concentration

Given the established size of the ROI, the SCM has been characterized when varying concentrations of the particle suspension affect the overall dispensing efficiency. Series of particle suspensions were prepared using different polystyrene bead concentrations ranging from 2.5×10^5 to 7.8×10^5 beads per ml and then printed onto glass slides as described before. As a noticeable result, it was found that (i) variations in particle density in the considered range have only a weak influence on the dispensing efficiency and (ii) the best dispensing efficiency of about 87% is obtained with the smallest concentration. With higher concentrations, the number of spots containing more than one bead increases, but never exceeds 5 beads per spot in the worst case scenario (Fig. 3).

3.4 Printing single adherent cells

To assess the SCM's performance for living biological cells, suspended HeLa (a cervical cancer cell line) cells were used. These cells are generally considered to be more fragile than CHO-cells, which have been used most often in cell printing studies to date. Thus, the selected cell line can be considered as a realistic model to test the performance of the method. Before starting the experiment to evaluate the viability of printed single cells, an evaluation for studying the single cell printing efficiency was performed by the same experiment as with polystyrene beads. The reasons behind are that (1) the viscosity of the cell culture media was approximately twice as high as for deionized water (culture media: 1.92 mPa s, DI-water: 0.98 mPa s—measured data not shown). Therefore it was vital to ensure that HeLa cell could be delivered and deposited comparable with polystyrene beads. (2) The cells used in this experiment were not labelled with any fluorescence molecule and furthermore the irregularities in size and shape for living cells were obvious compared with polystyrene beads. Therefore it was important to evaluate the capability of the algorithm to recognize real cells with the same approach like before. With the same setup as before, droplets of 400 pl could be dispensed using the dispensing parameters: maximum actuator displacement 8 μm and actuator extension velocity 40 μm ms^{-1}. Using the same ROI and the method as before, HeLa cells were printed on glass slides for varying cell concentrations.

The dispensing efficiency as shown in Fig. 4(a) was similar to that of the polystyrene beads. A high dispensing efficiency of 87% could also be obtained for HeLa cells in the best case. However, increasing the cell concentration significantly beyond 5.3×10^5 cells per ml had the effect of reducing the dispensing efficiency.

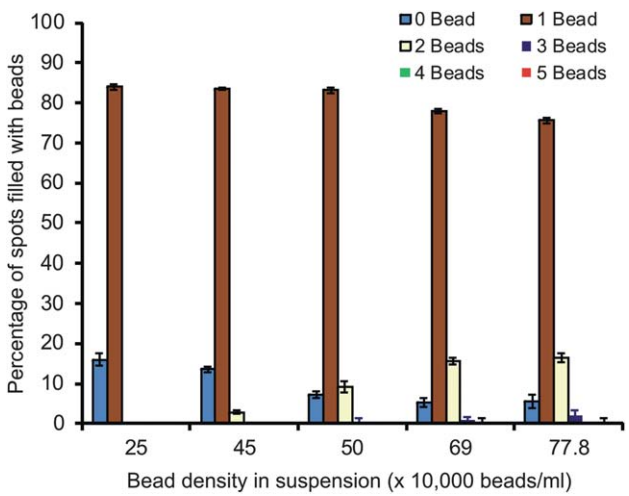

Fig. 3 Plot shows results for printing polystyrene beads on glass slides at different bead concentrations. All data correspond to a median from 50 printed spots.

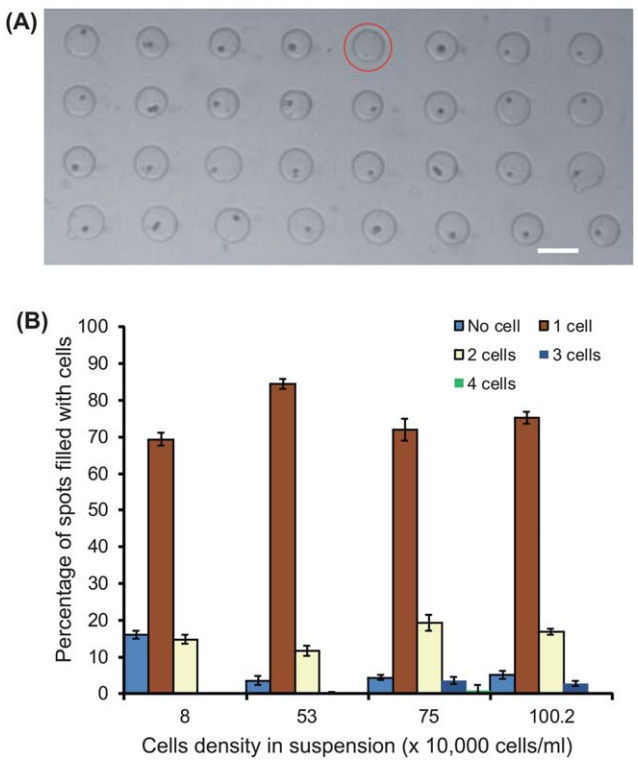

Fig. 4 (a) Micrograph at 4× objective magnification shows HeLa cells patterned on a glass slide to form 40 printed spots (8 × 4 array) containing one single HeLa cell each. The red circle marks a void spot. Scale bar 200 μm. (b) Comparison of the dispensing efficiency for HeLa cells printed on glass slide as a function of cell suspension concentration.

While the effects of changes in cell concentration seem to be more significant for the HeLa cells than for the microbeads, no significant influence of the cell concentration on the number of void spots can be detected. For subsequent experiments, the cell suspension density was prepared at 5.0×10^5 cells per ml.

3.5 Effect of actuator extension speed to the single cell viability

Apart from a high dispensing efficiency of course, the survival rate of cells being subjected to single cell manipulation is of the utmost importance. Therefore, the ability of the HeLa cells to survive throughout the printing process was assessed. One well known and important parameter that influences the viability of cells in liquid flows is the maximum shear rate that occurs in the flow. If this maximum shear rate is too high, it might damage the cell membrane or have other adverse effects on the cell viability. Though, the exact value of the maximum shear rate inside the dispenser chip could not be determined experimentally, its influence was studied. For the used dispenser chip, faster actuator extension velocities lead to higher flow rates and thus higher shear rates inside the nozzle. Therefore, by varying the actuator extension velocity, the shear rate inside the nozzle and the droplet velocity could be changed and the cell viability was studied as a function of it.

For the experiments, the dispensing parameters to obtain droplet volumes of 400 pl cell suspension were set to 8 μm maximum actuator displacement and the actuator extension velocity was varied from 30 μm ms^{-1} to 50 μm ms^{-1}. For each actuator extension velocity, single HeLa cells were printed into a microwell-plate and cultured over a course of time as outlined in the methods section. As expected, the dispensing efficiency does not show a significant change while varying the actuation velocity. Single HeLa cells were separated into individual wells where they at least doubled in cell count by cell division within 20 hours of incubation. After two days of incubation, the cells in each well were counted and the percentage viable cells calculated. At the slowest actuation velocity of 40 μm ms^{-1}, 75% of the seeded single-cells remained viable, but with increasing actuation velocity the viability decreased gradually (Fig. 5).

However, it is unlikely that this decrease is caused by the studied shear rate effect alone. For comparison, an ensemble of cells dispensed into one well by 20 droplets generated at identical parameters as shown in the control B did not show any effect of shear rate influence on the survival rate (*cf.* line plot in Fig. 5). Therefore, it has to be suspected that the mere isolation of the HeLa cells also contributes to the reduced survival rate and not only the shear rate experienced during the printing process. Since, an adverse effect of higher shear rate cannot be excluded based on the experimental data it is reasonable to assume that the optimum dispensing conditions to print single cells are obtained at the slowest actuation velocity that still can produce droplets.

3.6 Post-printing single cell growth

In further experiments, the growth of single cells printed under such optimum dispensing conditions into microwell plates was studied. To continuously monitor the cell growth after single cell printing, a microwell plate was populated with single cells as described before. Then arbitrarily, 20 wells were selected that contained a single cell which was still viable after one day. The

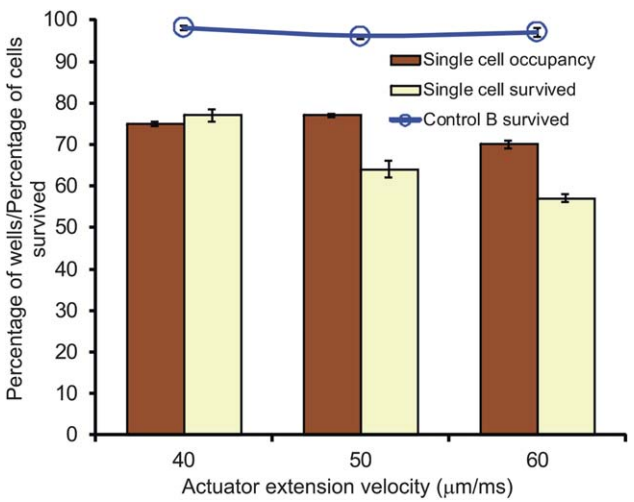

Fig. 5 Increasing the actuator extension velocity seems to decrease the single-cell survival rate. However, the viability trend in control B (cell ensemble printed by dispensing 20 × 400 pl droplets of cells suspension without controlling the cell number) shows that the cells proliferate independently of the actuator extension velocity. The data represent the median from 30 wells seeded with single cells after two days in culture.

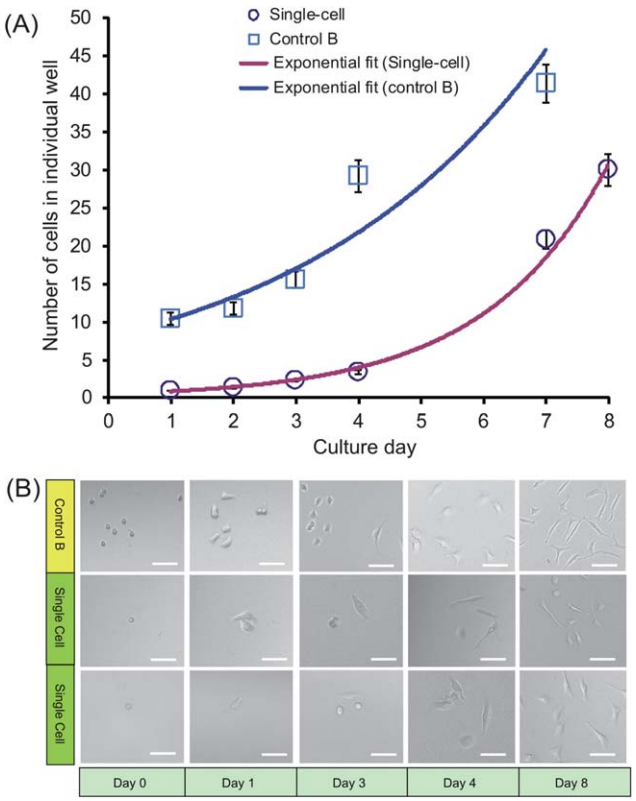

Fig. 6 (a) Number of cells in each well prepared initially with a single cell and tracked over 8 days in culture. The cells proliferated over time and the number of cells was fitted to an exponential function. The displayed data correspond to a median from 20 wells. (b) Examples of micrographs showing the cell condition in one of the "control B" wells and two "single cell populated" wells during selected days in culture. Scale bar, 50 μm.

well plate was then continuously incubated for the subsequent days and the selected wells were monitored over time by counting the cells in each well using a bright field microscope.

Interestingly, the cells divided constantly and showed a linear growth profile until day 3 as indicated in Fig. 6(a). On the subsequent days, the cells expanded exponentially and reached 10% confluence after eight days incubation (Fig. 6(b)). Monitoring the growth rate was stopped after day 11 where the cells reached almost 20% confluence.

These results have been compared with a control group of cells that was printed as an ensemble of cells into one well by dispensing 20 droplets of 400 pl each without controlling the number of cells in each droplet. This control group showed a very similar exponential growth to the populations that started from a single cell. In total these observations are a first "proof of principle" of the ability of the SCM to manipulate single adherent mammalian cells without significant loss of viability.

4. Discussion

The Single Cell Manipulator device presented in this study represents a major step forward in the area of single cell diagnostics, single cell therapeutics and cell and systems biology. The basis of this, is the recognition that the molecular trademarks of some diseases are best deciphered by the analysis of cell subpopulations on one level, and single cells on the next. The ability to print and reculture single cells in a positional manner, without major loss of viability, has huge implications for many diverse clinical applications.

Mechanical tissue microdissection methods such as laser capture microdissection provide a precise means of isolating single cells for gene expression profiling, and are often used to create discrete gene expression profiles of different cell types in a mixed tumour cell population. However, in the case of microdissection, such cells are rendered non-viable and no further downstream experiments can be performed. Single cell proteome analysis has been shown to be particularly useful in the stratification of solid tumours. In a recent analysis of glioblastoma multiforme, which is the most lethal form of adult brain cancer, multiparameter single cell signalling measurements were analysed for four critical signalling proteins of the oncogenic phosphoinositide 3-kinase (PI3K)/Akt/mammalian target of rapamycin (mTOR) signalling pathway.[25] In this study, single cell proteomics was performed using microfluidic imaging cytometry (MIC) and compared to standard immunohistochemistry for the four markers and together with the clinical data, this information was used to cluster patients according to clinical outcome and risk of progression. Single cell analysis may be used theranostically in the context of prenatal screening of foetal cells and in the analysis of circulating tumour cells for the detection of abnormal expression signatures.[2,3]

At the transcriptome level, single cell analysis applied to siRNA models has shown that within an siRNA treated cell line, distinct populations of varying knockdown efficiency may emerge.[26] Such disparity may not be accounted for in an overall calculation of % knockdown efficiency and can only be uncovered by performing gene expression analysis on single cells. Single cell analysis of a Jurkat cell line, showed that following silencing of GAPDH, two distinct cell lineages emerged: those with partial knockdown and those with complete knockdown. This segregation of cells based on GAPDH gene expression was masked when gene expression profiling was performed on greater numbers of cells.[26] Identification and confinement of particular cell types in systems will create microenvironments where single cell targeted siRNA interference can be performed. A recent study by Saito *et al.*, which used a single cell manipulation support, enabled femtoinjection of interfering RNA into a single mouse embryonic stem cell for quantitative analysis of transient gene expression.[27]

The SCM presented in this study may be adapted further to segregate cells according to the expression of optical fluorescent tags or by cellular electrical impedance measurements by the addition of a fluorescent recognition or electrical impedance module to the sorting algorithm. Such advances may allow the creation of cancer arrays and pre-cancer arrays where the cells of a clinical sample are spatially arranged according to a gradient of abnormality. This would assist in the creation of sequence and protein databases for individual cells of tumours of a particular disease state in a move towards genetically informed, personalised medicine.

The novelty of the presented method rests upon the ability of controlled encapsulation of single-cells within picolitre sized droplets and the non-contact printing of these droplets onto predefined locations at a reasonably high yield of up to 87% with considerable high survival rates of about 75% (determined for HeLa cells). Perhaps, this feature is a fundamental advance compared to existing non-contact techniques like inkjet printing of cells with random populations of cells per droplet. The obvious limitation of conventional inkjet print heads is the cell detection mechanism which is not present in these devices. Therefore, a sorting of droplets according to the number of encapsulated cells is not possible. However, in principle the described method could perform equally with any other dispenser which provides (i) a drop-on-demand dispensing mode and (ii) features a transparent nozzle which is accessible for optical imaging.

Of course, there are in principle various other possibilities to realize cell detection inside a droplet generating device without the use of optical imaging. For the presented method a computer vision system was selected, because it was rather simple to integrate with the existing transparent dispenser chip which was originally designed for applications other than dispensing living cells. Within the scope of the presented study, the basic working principle of the method could be proven by integrating the dispenser chip, the optical detection system, the control algorithm and a motion control system to perform the described experiments. The complete system ultimately provides a platform for single-cell manipulation that can be used and tested for separating, collecting and printing of single-cells for further downstream investigations.

The size and position of the ROI are the sensitive elements and determinant factors that contributed to the dispensing efficiency. Of course the point of measurement should be as close as possible to the point where the droplets are ejected to reduce any uncertainty. The decision to locate the ROI close to the nozzle is further grounded on the geometrical shape of the fluid channel that has a tapered constriction feature towards the nozzle. This geometrical shape generates a fluid flow focusing effect, which

narrows the fluid flow into smaller streams while approaching the nozzle section. As a consequence, the cell population is gradually reduced and the flow streams are aligned towards the nozzle orifice. Another contributing factor that affects the dispensing efficiency is the depth of the fluid channel. With a 40 μm deep channel like that used in the presented device and using HeLa cells with an average diameter of 12 μm, there is certain probability of more than one and up to three cells being stacked on top of each other along the channel depth. Such a situation can lead to false positive results by the single cell detection algorithm and is one possible reason for the dispensing efficiency not having reached higher values than 87% in this study.

If the cell density is sufficiently high to enable one cell per droplet in a statistical average, the single cell printing frequency mainly depends on how fast the image recognition algorithm can be executed and how fast the dispenser can be moved and triggered. Obviously, reducing the image size will reduce the software processing time and hence increase the printing frequency. To capture the ROI as defined in the previous section, an area of only 100 μm × 100 μm surrounding the nozzle was monitored at 3.2× objective magnification. The resulting image of 50 × 50 pixels size enabled sorting frequency of 8 events per second on average. Although the sorting performance is far below the well-established fluorescent activated cell sorter (FACS) technology, the SCM as described here can be regarded as a complementary technique for separating and manipulating single cells by non-contact printing. In particular, the method presented here is much more cost efficient than FACS and does not require any labelling. The main advantage compared to FACS technology is however that the single-cells can not only be sized and counted (which is a straightforward feature that was not exploited in this study), but can be separated in a very small volume of cell culture liquid and printed onto a wide range of substrates.

Conclusions

In conclusion, we have outlined a non-contact method for the controlled separation of single cells confined in a droplet that can be printed inkjet-like onto predefined locations. We validated experimentally the suitability of this method to manipulate adherent mammalian cells by performing experiments with HeLa cells. The achieved dispensing efficiency and the viability of the cells after printing suggest that the presented method is a suitable platform for printing single cells of various types for all kinds of biological studies. Single cell sorting combined with a single cell omic approach has the potential to revolutionise our understanding of systems biology in clinical diagnostics, therapeutics and theranostics.

Acknowledgements

The authors gratefully acknowledge support from Biofluidix GmbH, Germany for providing the BioSpot® 160 automation system; Department of Molecular Pathology, University of Dublin, Trinity College and Coombe Women and Infants University Hospital, Dublin, Ireland for providing HeLa cell samples. A.Y. thanks the Ministry of Higher Education, Malaysia for granting a graduate scholarship.

References

1 M. Toner and D. Irimia, *Annu. Rev. Biomed. Eng.*, 2005, **7**, 77–103.
2 M. Cristofanilli, G. T. Budd, M. J. Ellis, A. Stopeck, J. Matera, M. C. Miller, J. M. Reuben, G. V. Doyle, W. J. Allard, L. W. M. M. Terstappen and D. F. Hayes, *N. Engl. J. Med.*, 2004, **351**, 781–791.
3 K. Krabchi, F. Gros-Louis, J. Yan, M. Bronsard, J. Massé, J. C. Forest and R. Drouin, *Clin. Genet.*, 2001, **60**, 145–150.
4 T. C. Moloney, G. E. Rooney, F. P. Barry, L. Howard and E. Dowd, *Brain Res.*, 2010, **1359**, 33–43.
5 H. M. Shapiro, *Practical Flow Cytometry*, Wiley-Liss, 2003.
6 A. Folch and M. Toner, *Annu. Rev. Biomed. Eng.*, 2000, **2**, 227–256.
7 A. Azioune, M. Storch, M. Bornens, M. Thery and M. Piel, *Lab Chip*, 2009, **9**, 1640–1642.
8 J. Ziauddin and D. M. Sabatini, *Nature*, 2001, **411**, 107–110.
9 W. Xu, A. Luikart, C. Sims and N. Allbritton, *Anal. Bioanal. Chem.*, 2010.
10 J. R. Rettig and A. Folch, *Anal. Chem.*, 2005, **77**, 5628–5634.
11 T. Yoshiharu, K. Hiroyuki, K. Sachiko, H. Ritsu, T. Kazuto, M. Kazumi, O. Tatsuhiko, K. Shinichi, O. Tsutomu, F. Satoshi, T. Chise, T. Hideki, C. Kazuaki, Y. Katsutoshi, T. Eiichi, S. Toshiro and M. Atsushi, *Cytometry, Part A*, 2007, **71**, 1003–1010.
12 A. Rosenthal, A. Macdonald and J. Voldman, *Biomaterials*, 2007, **28**, 3208–3216.
13 P. Calvert, *Science*, 2007, **318**, 208–209.
14 U. Demirci and G. Montesano, *Lab Chip*, 2007, **7**, 1139–1145.
15 N. J. Suwan, N. Q. Amer and A. M. E. Peter, *Small*, 2006, **2**, 216–219.
16 T. Xu, J. Jin, C. Gregory, J. J. Hickman and T. Boland, *Biomaterials*, 2005, **26**, 93–99.
17 B. Thomas, X. Tao, D. Brook and C. Xiaofeng, *Biotechnol. J.*, 2006, **1**, 910–917.
18 M. Nakamura, A. Kobayashi, F. Takagi, A. Watanabe, Y. Hiruma, K. Ohuchi, Y. Iwasaki, M. Horie, I. Morita and S. Takatani, *Tissue Eng.*, 2005, **11**, 1658–1666.
19 J. W. Cris Wilson and B. Thomas, *Anat. Rec., Part A*, 2003, **272**, 491–496.
20 T. Xu, H. Kincaid, A. Atala and J. J. Yoo, *J. Manuf. Sci. Eng.*, 2008, **130**, 021017–021015.
21 N. Hey, M. Freygang, H. Gruhler, H. Sandmaier and R. Zengerle, in *MicroElectro Mechanical Systems, 1998. MEMS 98. Proceedings. The Eleventh Annual International Workshop on*, 1998, pp. 429–431.
22 A. Yusof, L. Riegger, N. Paust, A. Ernst, R. Zengerle and P. Koltay, in *Actuator 2010*, WFB Wirtschaftförderung Bremen GmbH, Bremen, Germany, 2010, pp. 1033–1036.
23 R. Jain, R. Kasturi and B. G. Schunck, *Machine Vision*, McGraw-Hill, 1995.
24 R. E. Saunders, J. E. Gough and B. Derby, *Biomaterials*, 2008, **29**, 193–203.
25 J. Sun, M. D. Masterman-Smith, N. A. Graham, J. Jiao, J. Mottahedeh, D. R. Laks, M. Ohashi, J. DeJesus, K.-i. Kamei, K.-B. Lee, H. Wang, Z. T. F. Yu, Y.-T. Lu, S. Hou, K. Li, M. Liu, N. Zhang, S. Wang, B. Angenieux, E. Panosyan, E. R. Samuels, J. Park, D. Williams, V. Konkankit, D. Nathanson, R. M. van Dam, M. E. Phelps, H. Wu, L. M. Liau, P. S. Mischel, J. A. Lazareff, H. I. Kornblum, W. H. Yong, T. G. Graeber and H.-R. Tseng, *Cancer Res.*, 2010, **70**, 6128–6138.
26 S. M. Chan, J. A. Olson and P. J. Utz, *Cytometry, Part A*, 2006, **69**, 59–65.
27 H. Matsuoka, S. Shimoda, M. Ozaki, H. Mizukami, M. Shibusawa, Y. Yamada and M. Saito, *Biotechnol. Lett.*, 2007, **29**, 341–350.

